JOURNAL OF COMPUTATIONAL PHYSICS **125,** 124–134 (1996)
ARTICLE NO. 0083

Contribution to the Optimal Shape Design of Two-Dimensional Internal Flows with Embedded Shocks

ANGELO IOLLO*

Dipartimento di Ingegneria Aeronautica e Spaziale, Politecnico di Torino, 10129 Turin, Italy

AND

MANUEL D. SALAS

NASA Langley Research Center, Hampton, Virginia 23681-0001

Received December 9, 1994; revised August 28, 1995

We explore the praticability of optimal shape design for flows modeled by the Euler equations. We define a functional whose minimum represents the optimality condition. The gradient of the functional with respect to the geometry is calculated with the Lagrange multipliers, which are determined by solving a *costate* equation. The optimization problem is then examined by comparing the performance of several gradient-based optimization algorithms. In this formulation, the flow field can be computed to an arbitrary order of accuracy. Finally, some results for internal flows with embedded shocks are presented, including a case for which the solution to the inverse problem does not belong to the design space. © 1996 Academic Press, Inc.

1. INTRODUCTION

A classical problem in engineering is to define the shape of a manufacture to achieve a required performance. In fluid dynamics, techniques have been developed to solve the following inverse problem: given a pressure or a velocity distribution over an aerodynamic body, determine the corresponding geometry. See, for example, reference [7]. A broader category of problems can be solved by means of optimization, provided that one is ready to accept the necessity of computing the flow field hundreds of times.

It is possible, in fact, to define a functional or cost function such that its minimum represents an optimal solution. For example, the drag of an airfoil can be selected as the cost function to be minimized for a given lift. Many existing methods of solving such minimization problems are based on descent algorithms which make use of the gradient of the functional with respect to the geometry. The gradient is usually calculated with a black-box method. Such a method consists in using finite differences to determine the gradient of the functional, and therefore, for each gradient computation, it needs as many flow-field solutions as the number of design variables.

In using models of increased complexity to describe the flow field, such as Euler or Navier–Stokes equations, the development of new algorithms is necessary to reduce the computational load. In this paper, we investigate one method for achieving this reduction.

The cost of the optimization comes from three sources. The cost of evaluating the flow field, the cost of evaluating the gradient and number of gradient evaluations necessary to reach the minimum. In this article we are concerned with the problem of avoiding unnecessary computations for the evaluation of the gradient of the functional with respect to the design variables. Other methods, including the black-box method and the sensitivity equation method [2], require the solution either of the Euler equations or of an additional partial differential equation (PDE) for each design variable and for each gradient evaluation.

We apply a variational technique that has been used since before complex flows could be integrated numerically. See, for example, Ref. [9]. Jameson [6] was the first to apply the abovementioned technique to computational fluid dynamics. With such an approach, a functional or cost function is determined such that its minimum represents an optimal solution. The flow-field equations can be considered as constraints in the minimization. By introducing a set of Lagrange multipliers, the constrained minimum of the functional with respect to the geometry, is transformed into a free minimum with respect to the geometry to the flow-field unknowns, and to the Lagrange multipliers.

With this formulation the gradient of the functional can be calculated with respect to the geometry by computing the flow field only once for each gradient evaluation. For

* This research was supported in part under NASA contract no. NAS1-19480 while the first author was in residence at the Institute for Computer Applications in Science and Engineering, NASA Langley Research Center, Hampton, VA 23681-0001.

0021-9991/96 $18.00
Copyright © 1996 by Academic Press, Inc.
All rights of reproduction in any form reserved.

incompressible irrotational steady flows, a further reduction in the computational effort is possible (see [13]).

The formulation developed in this work is in the spirit of the mathematical frame set in [8]. In fact, calculating the gradient of the functional, the flow-field variables are considered independent of the geometry, thus avoiding inaccuracies and confusions that may arise when considering the variation of the geometry. Although this formulation is similar to that in [6], it circumvents the theoretical objection of adding to the functional to be minimized a term that is always zero if the flow-field equations are satisfied. Compared to previous work, our formulation is not tied to conformal mapping and can treat captured or fitted shocks.

In this respect, we extend the work presented in Ref. [1]. In that formulation, an exact gradient with respect to the design variables was obtained for the discretized functional. This is a limitation for compressible flows, because in presence of shocks the discretized functional could present discontinuities. However, in paper [1], only reversible nozzle flows were taken into account.

In reference [5] quasi one-dimensional compressible flows with embedded shocks were considered and the gradient of the functional was derived on a continuous level. Here, we consider two-dimensional Euler flows with shocks, and we provide a method for calculating the conditions that the Lagrange multipliers must satisfy at the boundaries and at the shock. Finally, we point out that our formulation can be used with complex flow solvers because the differentiability of the solver is not requested.

2. PROBLEM STATEMENT

The Euler equations are given by

$$\mathbf{U}_t + \mathbf{F}_x + \mathbf{G}_y = \mathbf{0}, \tag{1}$$

where

$$\mathbf{U} = \begin{pmatrix} \rho \\ \rho u \\ \rho v \\ \rho e \end{pmatrix} \mathbf{F} = \begin{pmatrix} \rho u \\ p + \rho u^2 \\ \rho uv \\ u(\rho e + p) \end{pmatrix} \mathbf{G} = \begin{pmatrix} \rho v \\ \rho uv \\ p + \rho v^2 \\ v(\rho e + p) \end{pmatrix}$$

with

ρ = density

u = x component of velocity vector

v = y component of velocity vector

e = specific total energy

p = pressure

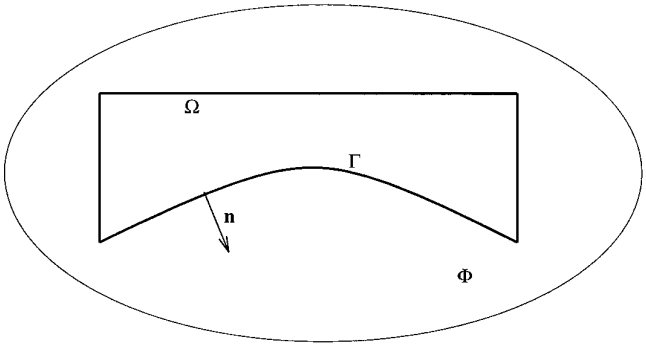

FIG. 1. Model problem.

a = speed of sound

γ = specific heats ratio

$$\kappa = \frac{\gamma - 1}{2}$$

and $p = \kappa\rho(2e - u^2 - v^2)$. Furthermore,

$$\mathbf{F} = \frac{\partial \mathbf{F}}{\partial \mathbf{U}} \mathbf{U} = \mathbf{A}(\mathbf{U})\mathbf{U} \tag{2}$$

and

$$\mathbf{G} = \frac{\partial \mathbf{G}}{\partial \mathbf{U}} \mathbf{U} = \mathbf{B}(\mathbf{U})\mathbf{U}, \tag{3}$$

where $\mathbf{A}$ and $\mathbf{B}$ are given in Appendix I.

We assume that these equations are defined on a physical space Φ. In this space is included a subdomain Ω whose boundary is denoted by Γ. On the boundary, we define a curvilinear coordinate s and a normal $\mathbf{n} = (n_x, n_y)$ that points outward.

The optimization problem studied here is defined as the minimization of the functional $\mathscr{E} = \int_\Gamma \phi(p, \rho, u, v, \Gamma)\, ds$ over all admissible shapes of the subdomain Ω, subject to the steady-state Euler equations with proper boundary conditions on Γ.

Although the method we present is general, we focus on the following model problem. The subdomain Ω is represented by a nozzle. (See Fig. 1.) At the inlet, total pressure, total temperature, and the ratio $\sigma = v/u$ are fixed. At the outlet, if the flow is subsonic, the static pressure is fixed, and at the solid walls the impermeability condition $un_x + vn_y = 0$ is enforced. The upper wall is kept fixed. The lower wall Θ is represented by the parameterization

$$y(\Theta) = \sum_i \alpha_i f_i(x), \tag{4}$$

where the functions $f_i(x)$ are shape functions and $\alpha = (\alpha_1, ..., \alpha_i, ...)$ is the corresponding set of shape coefficients. Given a desirable lower wall pressure distribution $p^*(x)$ and the actual pressure distribution on the lower wall $p^w(x)$, the optimization problem consists in finding a set of shape coefficients α_i such that the functional

$$\mathscr{E} = \frac{1}{2}\int_a^b (p^w - p^*)^2\, dx \tag{5}$$

is minimized.

3. LAGRANGE MULTIPLIERS AND OPTIMALITY

The problem of achieving the minimum is addressed by introducing a set of Lagrange multipliers. Consider the augmented functional

$$\begin{aligned}\mathscr{L}(\mathbf{U}, \alpha, \mathbf{\Lambda}, \mu) = \mathscr{E} &+ \int_\Omega \mathbf{\Lambda}(\mathbf{A}\mathbf{U}_x + \mathbf{B}\mathbf{U}_y)\, d\Omega \\ &+ \int_\Theta \mu\rho\mathbf{V}\cdot\mathbf{n}\, ds,\end{aligned} \tag{6}$$

where $\mathbf{V} = (u, v)$. The vector $\mathbf{\Lambda}(x, y) = {}^t(\lambda_1, \lambda_2, \lambda_3, \lambda_4)$ and the scalar $\mu(s)$ are the continuous equivalents of the Lagrange multipliers.

We calculate the variation of the functional $\mathscr{L}$ with respect to the variation of the functions $\mathbf{U}$, $\mathbf{\Lambda}$, and μ and the parameters α_i, respectively. When $\mathbf{U}(x, y)$ is increased by a function $\varepsilon\tilde{\mathbf{U}}(x, y)$, the functional $\mathscr{L}$ increases by an amount $\varepsilon\delta\mathscr{L}_U$. In the same way, $\mathbf{\Lambda}(x, y)$ is increased by $\varepsilon\tilde{\mathbf{\Lambda}}(x, y)$; $\mu(s)$, by $\varepsilon\tilde{\mu}(s)$; and each α_i, by $\varepsilon\tilde{\alpha}_i$.

If we follow the derivation in Appendix II and take

$$\delta\mathscr{L} = \delta\mathscr{L}_U + \delta\mathscr{L}_\Lambda + \delta\mathscr{L}_\mu + \delta\mathscr{L}_\alpha$$

then we obtain

$$\begin{aligned}\delta\mathscr{L}_U = &\int_a^b \left.\frac{\partial p}{\partial \mathbf{U}}\right|_\Theta (p^w - p^*)\tilde{\mathbf{U}}\, dx + \int_\Gamma {}^t\mathbf{\Lambda}(\mathbf{A}n_x + \mathbf{B}n_y)\tilde{\mathbf{U}}\, ds \\ &- \int_\Omega ({}^t\mathbf{\Lambda}_x\mathbf{A} + {}^t\mathbf{\Lambda}_y\mathbf{B})\tilde{\mathbf{U}}\, d\Omega + \int_\Theta \mu\mathbf{n}\frac{\partial\rho\mathbf{V}}{\partial\mathbf{U}}\tilde{\mathbf{U}}\, ds,\end{aligned} \tag{7}$$

where

$$\frac{\partial p}{\partial \mathbf{U}} = 2k\left(\frac{u^2+v^2}{2}, -u, -v, 1\right) \quad \text{and} \quad \frac{\partial\rho\mathbf{V}}{\partial\mathbf{U}} = \begin{pmatrix} 0 & 1 & 0 & 0 \\ 0 & 0 & 1 & 0 \end{pmatrix}.$$

Furthermore,

$$\delta\mathscr{L}_\Lambda = \int_\Omega {}^t\tilde{\mathbf{\Lambda}}(\mathbf{A}\mathbf{U}_x + \mathbf{B}\mathbf{U}_y)\, d\Omega \tag{8}$$

$$\delta\mathscr{L}_\mu = \int_\Theta \tilde{\mu}\rho\mathbf{V}\cdot\mathbf{n}\, ds \tag{9}$$

$$\begin{aligned}\delta\mathscr{L}_\alpha = \sum_i \Bigg[&\int_a^b \left.\frac{dp}{dy}\right|_\Theta (p^w - p^*) f_i\, dx \\ &+ \int_\Theta {}^t\mathbf{\Lambda}(\mathbf{A}\mathbf{U}_x + \mathbf{B}\mathbf{U}_y) f_i \cos\theta\, ds \\ &+ \int_\Theta \mu\frac{\partial(\rho\mathbf{V})}{\partial y}\cdot\mathbf{n} f_i\, ds - \int_\Theta \mu\rho\mathbf{V}\cdot\mathbf{t}\frac{df_i}{dx}\cos^2\theta\, ds \\ &+ \int_\Theta \mu\rho\mathbf{V}\cdot\mathbf{n}\frac{df_i}{dx}\sin\theta\cos\theta\, ds\Bigg]\tilde{\alpha}_i,\end{aligned} \tag{10}$$

where θ is the angle between the normal $\mathbf{n}$ and the y-axis and $\mathbf{t} = (-n_y, n_x)$.

At the minimum of the functional, we have $\delta\mathscr{L} = 0$ for all possible choices of the functions $\tilde{\mathbf{U}}$, $\tilde{\mathbf{\Lambda}}$, and $\tilde{\mu}$ and of the parameters $\tilde{\alpha}$. This condition is reached when

$$\delta\mathscr{L}_U = \delta\mathscr{L}_\Lambda = \delta\mathscr{L}_\mu = \delta\mathscr{L}_\alpha = 0. \tag{11}$$

Note that because of the necessary conditions (Eqs. (11)) the unconstrained minimum of the functional $\mathscr{L}(\mathbf{U}, \alpha, \mathbf{\Lambda}, \mu)$ corresponds to the constrained minimum of the functional $\mathscr{E}(\alpha)$. In fact, we have

$$\delta\mathscr{L}_\Lambda = 0 \Rightarrow \mathbf{A}\mathbf{U}_x + \mathbf{B}\mathbf{U}_y = \mathbf{0} \quad \text{and} \quad \delta\mathscr{L}_\mu = 0 \Rightarrow \rho\mathbf{V}\cdot\mathbf{n} = 0,$$

which means that $\mathbf{U}$ must satisfy the Euler equations with boundary conditions. In addition, for the minimum of $\mathscr{L}$, we have $\delta\mathscr{L}_U = 0$, which leads to

$${}^t\mathbf{A}\mathbf{\Lambda}_x + \mathbf{B}\mathbf{\Lambda}_y = \mathbf{0} \text{ on } \Omega \tag{12}$$

$$\begin{aligned}&\left.\frac{\partial p}{\partial \mathbf{U}}\right|_\Theta (p^w - p^*)\cos\theta + {}^t\mathbf{\Lambda}(\mathbf{A}n_x + \mathbf{B}n_y) \\ &\quad + \mu\mathbf{n}\frac{\partial\rho\mathbf{V}}{\partial\mathbf{U}} = \mathbf{0} \quad \text{on } \Theta.\end{aligned} \tag{13}$$

At the inlet, outlet, and upper wall,

$${}^t\mathbf{\Lambda}(\mathbf{A}n_x + \mathbf{B}n_y)\tilde{\mathbf{U}} = 0. \tag{14}$$

Given $\mathbf{U}$ and the set of costate equations (12) and (14), we can uniquely determine $\mathbf{\Lambda}$ in Ω and μ on Θ. (See Appendix III.)

Finally, given α and given $\mathbf{U}$ and $\mathbf{\Lambda}$ from the above equations, we can calculate from Eq. (10)

$$\begin{aligned}\frac{\partial \mathcal{L}}{\partial \alpha_i} = &\int_a^b \left.\frac{dp}{dy}\right|_\Theta (p^w - p^*) f_i \, dx \\ &+ \int_\Theta {}^t\mathbf{\Lambda}(\mathbf{A}\mathbf{U}_x + \mathbf{B}\mathbf{U}_y) f_i \cos\theta \, ds \\ &+ \int_\Theta \mu \frac{\partial(\rho \mathbf{V})}{\partial y} \cdot \mathbf{n} f_i \, ds - \int_\Theta \mu \rho \mathbf{V} \cdot \mathbf{t} \frac{df_i}{dx} \cos^2\theta \, ds \\ &+ \int_\Theta \mu \rho \mathbf{V} \cdot \mathbf{n} \frac{df_i}{dx} \sin\theta \cos\theta \, ds.\end{aligned} \tag{15}$$

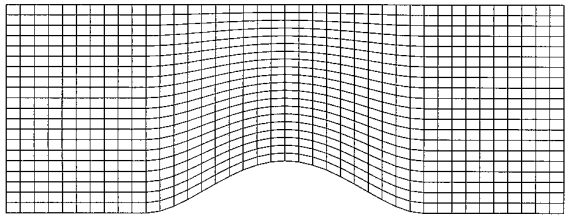

FIG. 2. Discrete grid.

In cases for which shock occurs in the flow field, we split the domain of integration by means of a curve Υ that coincides with the shock where it exists. Then, we follow the same derivation so far on each of the two subdomains, with Υ as a boundary. Considering the one-dimensional characteristic pattern of the costate equations in the direction normal to the shock, it is seen that the costate equations need additional conditions at the shock for the well posedness of the problem. For a complete discussion of this topic we refer the reader to [5]. The conditions derived for the two-dimensional case are presented in Appendix III.

The strategy that we use to achieve the minimum of $\mathcal{L}$ is as follows:

1. Start with a set α of shape coefficients.
2. Enforce $\delta\mathcal{L}_\Lambda = 0$ and $\delta\mathcal{L}_\mu = 0$ by finding $\mathbf{U}$ such that it satisfies the steady-state Euler equations and boundary conditions.
3. Enforce $\delta\mathcal{L}_U = 0$ by finding $\mathbf{\Lambda}$ such that it satisfies the costate equations and boundary conditions.
4. Calculate $\nabla_\alpha \mathcal{L}$. If $\nabla_\alpha \mathcal{L} = 0$ then we have determined the minimum; otherwise continue to steps 5 and 6.
5. Update α with criteria based on $\nabla_\alpha \mathcal{L}$.
6. Restart from step 2.

As anticipated in the Introduction, the cost of the optimization comes from three sources: the cost of evaluating the flow field, the cost of evaluating the gradient, and the number of gradient evaluations necessary to reach the minimum. With the above algorithm, we address the problem of reducing the cost of each gradient computation, because only one flow-field evaluation is necessary to compute all the components of the gradient, at the cost of solving the costate equations.

In contrast, for each gradient evaluation, the black-box method needs as many flow-field evaluations as the number of design variables, and the information it delivers is often inaccurate. Other existing methods, such as sensitivity equation methods (see [2]), offer more accurate gradient computations but suffer from the disadvantage of requiring the solution of PDE for each design variable. With such approaches, for a given number N of shape coefficients and for a given descent method, the cost of the minimization is about N times the cost of a minimization performed with the algorithm presented above, making many optimizations infeasible because too expensive.

4. DISCRETE PROBLEM

We introduce a discrete grid that is defined as $(x_l, y_m) = (x_0 + l\,\Delta x, y(\Theta) + m\,\Delta y)$, where Δx is constant and Δy is a constant fraction of the local height of the nozzle. (See Fig. 2.)

The steady solution of the Euler equations is obtained with a time-dependent technique, in the frame of an explicit finite-volume code. The conservative variables $\mathbf{U}$ are computed at the cell centers, and the fluxes $\mathbf{F}$ and $\mathbf{G}$ are evaluated at the cell interfaces with the approximate Riemann solver in Ref. [12]. Second-order accuracy is achieved by using an essentially nonoscillatory scheme [4]. With such an approach the flow-field values at the cell interfaces, used as initial conditions for the Riemann problem, are reconstructed by means of a linear interpolation. The occurrence of spurious oscillations is prevented using a minmod limiter. The amplitude of the integration step is chosen in accordance with the Courant–Friedrichs–Lewy (CFL) condition.

The costate equations are discretized on the same grid presented above. Because they have no conservative form, the numerical solution is obtained with a finite-difference scheme. We introduce a set of curvilinear coordinates $\varphi(x, y)$ and $\psi(x, y)$. The costate equations are then written

$${}^t\mathcal{A}\mathbf{\Lambda}_\varphi + {}^t\mathcal{B}\mathbf{\Lambda}_\psi = \mathbf{0}, \tag{16}$$

where $\mathcal{A} = \mathbf{A}\varphi_x + \mathbf{B}\varphi_y$ and $\mathcal{B} = \mathbf{A}\psi_x + \mathbf{B}\psi_y$. The transformations φ and ψ are defined as $(x_l, y_m) \xrightarrow{\varphi} l$ and $(x_l, y_m) \xrightarrow{\psi} m$, respectively.

We find the solution of Eq. (16) as the asymptotic limit of a *time-dependent* technique. As for the solution of the Euler equations, the CFL condition limits the convergence rate to the steady solution. Nevertheless, comparisons between time-iterative methods and direct solvers have shown that their overall costs (including memory) is similar

for two-dimensional problems and time-iterative methods are more efficient for three-dimensional problems.

Consider Eq. (16) embedded in time as

$$\pm \mathbf{\Lambda}_t + {}^{\mathrm{t}}\mathscr{A}\mathbf{\Lambda}_\varphi + {}^{\mathrm{t}}\mathscr{B}\mathbf{\Lambda}_\psi = \mathbf{0}. \tag{17}$$

We must select the proper sign for the time derivative. The inlet and outlet boundary conditions for the costate equations are complementary to those of the flow-field equations, in the sense that if the number of boundary conditions for the flow field is c, then the number of boundary conditions for the costate equations is $4 - c$. Therefore, the above equations and boundary conditions are well posed if we select the negative sign for the time derivative. In fact, the resulting characteristic pattern is mirror symmetric with respect to that of the flow-field equations.

In the presence of a shock in the flow field, the matrices ${}^{\mathrm{t}}\mathscr{A}$ and ${}^{\mathrm{t}}\mathscr{B}$ are discontinuous. In particular, the characteristic pattern at the shock indicates the necessity of a boundary condition for the costate equations. For further discussion, see Ref. [5].

The costate equations are linear and as such are the boundary conditions. We exploit this property to solve these equations numerically. Suppose that locally we separate the variables through the following approximation:

$$\mathbf{\Lambda}(\varphi, \psi, t) = \mathbf{\Lambda}'(\varphi, t) + \mathbf{\Lambda}''(\psi, t). \tag{18}$$

This separation of variables means that, for example, in a Taylor expansion about the point (φ, ψ) we disregard all terms that involve the cross product $\varphi\psi$ arising from terms higher than the first. This approximation is at least first-order accurate. We substitute Eq. (18) into Eq. (17) to obtain

$$-\mathbf{\Lambda}'_t - \mathbf{\Lambda}''_t + {}^{\mathrm{t}}\mathscr{A}\mathbf{\Lambda}'_\varphi + {}^{\mathrm{t}}\mathscr{B}\mathbf{\Lambda}''_\psi = 0$$

and we are left with the following subproblems in one dimension:

$$-\mathbf{\Lambda}'_t + {}^{\mathrm{t}}\mathscr{A}\mathbf{\Lambda}'_\varphi = \mathbf{0} \tag{19}$$

$$-\mathbf{\Lambda}''_t + {}^{\mathrm{t}}\mathscr{B}\mathbf{\Lambda}''_\psi = \mathbf{0}. \tag{20}$$

Let us define $\mathbf{n}_\varphi = (\varphi_x/\sqrt{\varphi_x^2 + \varphi_y^2}, \varphi_y/\sqrt{\varphi_x^2 + \varphi_y^2})$ and $\mathbf{n}_\psi = (\psi_x/\sqrt{\psi_x^2 + \psi_y^2}, \psi_y/\sqrt{\psi_x^2 + \psi_y^2})$. The left and right eigenvector matrices of $\mathscr{A}$ and $\mathscr{B}$ are calculated by using the formulas in Appendix I with $\mathbf{n} = \mathbf{n}_\varphi$ and $\mathbf{n} = \mathbf{n}_\psi$, respectively. After Eqs. (19) and (20) are diagonalized, we upwind the derivatives of the characteristic variables according to the signs of the corresponding eigenvalues. The time step Δt is chosen according to the CFL condition. This method can be regarded as a two-dimensional interpretation of the method presented in Ref. [10].

The boundary conditions can be split in a similar way. Consider, for example, the boundary condition at the solid wall. Because Eq. (19) is defined along the wall, the characteristic variables can be upwinded according to the corresponding eigenvalues. In contrast, the third row of Eq. (20), which corresponds to the characteristic with a speed of $+a$, is replaced by the boundary condition in Eq. (AIII.5). Note that the contravariant component of the speed in the direction ψ is 0; therefore, the resulting system can be written as

$$\begin{cases} \Delta^t W''_1 = 0 \\ \Delta^t W''_2 = 0 \\ n_x\,\Delta^{\mathrm{t}}\lambda''_2 + n_y\,\Delta^{\mathrm{t}}\lambda''_3 = -(p^w - p^*)\cos\theta - n_x\,\Delta^t\lambda'_2 - n_y\,\Delta^{\mathrm{t}}\lambda'_3 \\ \Delta^{\mathrm{t}} W''_4 = a\,\Delta t\,(\sqrt{\psi_x^2 + \psi_y^2})\,\Delta^m W''_4, \end{cases} \tag{21}$$

where $\Delta(\cdot)$ is the forward finite increment of the function $(\cdot)$ with respect to the superscripted variable and

$$\Delta\mathbf{W} = \begin{pmatrix} \Delta W_1 \\ \Delta W_2 \\ \Delta W_3 \\ \Delta W_4 \end{pmatrix} = {}^{\mathrm{t}}\mathbf{L}_n^{-1}\,\Delta\mathbf{\Lambda}.$$

In the third row of Eq. (21), we have the functions of $\Delta^{\mathrm{t}}\mathbf{\Lambda}'$, which are computed separately as mentioned. The other boundary conditions are enforced in the same pattern that is presented above.

In addition to the theoretical difficulties arising when flows with embedded shocks are considered, on the discrete level it is necessary to acquire the position of the shock. Although explicit treatment of shocks has been the subject of many papers (see for example [11]), we use a very simple and effective shock detection scheme. It is based on the assumption that the shock is represented, for example, by a grid curve $\psi = constant$. If this is the case, then it is enough to decompose the flow in the direction normal and tangent to this curve all over the flow field, checking if one of the acoustic signals speed relative to the normal flow is changing sign across two adjacent volumes. If the signs of these speeds are such that the corresponding characteristics are impinging, then we label that volume as one corresponding to the shock.

In general, the assumption that the shock overlaps a curve $\psi = constant$ is not always verified, unless some adaptive grid algorithm is used. In presence of shocks which are not parallel to the grid, the above algorithm

might fail to detect the shock. However for these cases the costate equations would still converge because their one-dimensional projections do not need any additional condition, as it is seen considering the characteristic pattern for these cases. In this respect, the solution of the costate equations is affected by the calculation of the shock position in the sense that unless the proper position is chosen, the costate equation *time-dependent* technique does not converge in the presence of shocks.

5. OPTIMIZATION EXPERIMENTS

The optimization problem is addressed with four different gradient-based criteria.

1. Steepest descent (SD1). The shape coefficients are updated as follows: $\alpha_i \leftarrow \alpha_i - v(\partial \mathscr{L}/\partial \alpha_i)$, where v is a given parameter.

2. Steepest descent with v selected as follows (SD2). Because we know the gradient $\nabla_\alpha \mathscr{L}$ at the present iteration, we can use a tentative step length v and can compute the gradient $\nabla_\alpha \mathscr{L}'$. By calculating $\nabla_\alpha \mathscr{L} \cdot \nabla_\alpha \mathscr{L}'$, we linearly estimate v such that eventually $\nabla_\alpha \mathscr{L} \cdot \nabla_\alpha \mathscr{L}'' = 0$. Each step of the optimization requires solution of the flow field and costate equations twice.

3. The BFGS algorithm (presented in Ref. [3]). This algorithm (BFGS1) accounts for the curvature of the hypersurface $\mathscr{L}$ representing the functional in the design space. The shape coefficients are updated according to the formula $\alpha_i \leftarrow \alpha_i - v d_i$, where $d = (..., d_i, ...)$ is the descent direction determined by $\mathbf{d} = \mathbf{H}\, \nabla_\alpha \mathscr{L}$ and $\mathbf{H}$ is an estimate of the inverse of the Hessian of the functional.

4. The BFGS algorithm (as above) with a linear estimate of v such that $\mathbf{d} \cdot \nabla_\alpha \mathscr{L}'' = 0$. Each optimization step requires solution of the flow field and costate equations twice (BFGS2).

The computations are performed on a 40×20 grid unless otherwise specified. Total pressure and total temperature at the inlet are taken unitary and $\sigma(0, y) = 0$. At the outlet, the static pressure depends on the test case considered. For the lower wall ordinate $y(\Theta)$, we have

$$y(\Theta) = \begin{cases} 0 & \text{if } -0.5 \le x < 0 \\ \displaystyle\sum_{i=1}^{4} \alpha_i x^{i+1}(x-1)^2 & \text{if } 0 \le x < 1 \\ 0 & \text{if } 1 \le x < 1.5. \end{cases}$$

The optimization consists in finding the four shape coeffi-

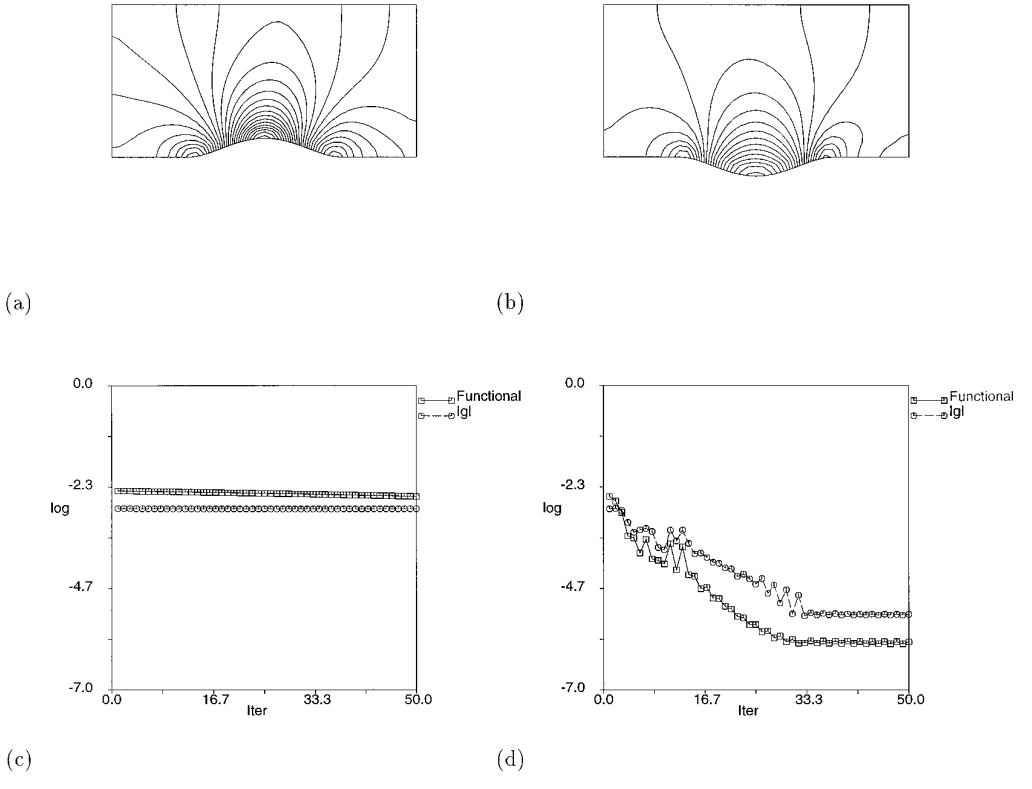

FIG. 3. (a) Target Mach number field; (b) starting configuration; (c) functional and modulus of gradient versus number of iterations for SD1; (d) BFGS2.

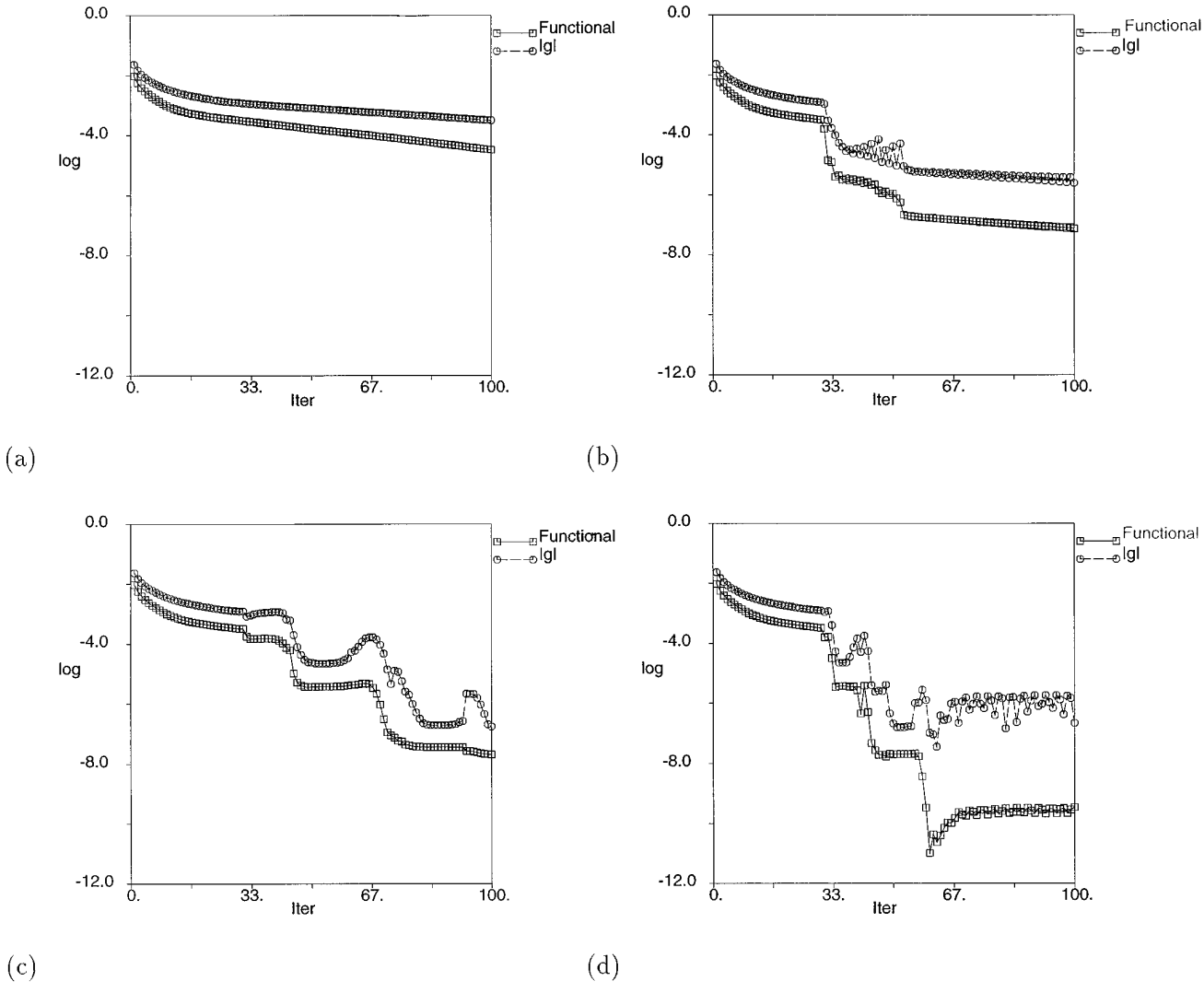

FIG. 4. (a) SD1; (b) SD2; (c) BFGS1; (d) BFGS2.

cients α_i such that the modulus of the gradient $\nabla_\alpha \mathscr{L}$ is 0. The *time-dependent* solutions to flow-field and costate equations are considered steady when the residuals are less than 10^{-5}.

We first devote our attention to the following test case: recover a pressure distribution in a subsonic nozzle flow where the outlet pressure is 0.9 referred to inlet total pressure. We take $\alpha = (2,0,0,0)$ and define the corresponding configuration as the optimal configuration. Then, we compute the flow field and determine the pressure distribution on the lower wall. This pressure distribution p^* is the one we want to recover with the optimization algorithm. In Fig. 3, the target flow field and the starting configuration, obtained with $\alpha = (-2,0,0,0)$, are shown along with the convergence histories for SD1 and BFGS2.

For the supersonic case, we take a constant section channel as a starting configuration and $\alpha = (2,0,0,0)$ as the target. In Fig. 4, we present the results obtained when the outlet pressure is lowered to 0.5 of the inlet total pressure. A relevant shock is present in the target flow field, as is seen in Fig. 5. In the first optimization iterations, we updated the shape coefficients as was done for SD1. This step is necessary because this far from the minimum the functional $\mathscr{L}$ might be not convex; therefore, the estimate of v used in BFGS2 and SD2 might not be correct. Figure 6 shows the sequence of lower wall configurations obtained with BFGS2. The optimal wall and the target wall overlap.

In all the examples in which the SD2 or the BFGS2 strategies were employed, both the gradient and the functional suffered from small oscillations, despite the final convergence to the minimum. The SD2 and BFGS2 algo-

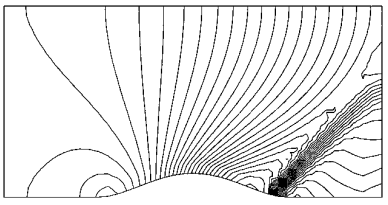

FIG. 5. Target Mach number field.

rithms estimate the step as is explained above. This estimate can be too large, therefore these two algorithms are more subject to fluctuations. Even the SD1 and BFGS1 algorithm are monotonic decreasing sequences only if there is an exact line search in the direction chosen. Since we take a constant step, the decrease of the functional may be not guaranteed. Furthermore, when a shock is present in the flow field, the functional may suffer from jumps due to the discrete displacement of the discontinuity through the grid.

In Fig. 4(d) it can be noticed that the solution is settled out after 70 iterations. On the way to the minimum, the functional reaches values lower than the final one. This is due to the fact that the minima of the analytic functional and of the discretized one may differ.

The second test case is designed to check the capability of the algorithm in detecting minima in cases for which the desired pressure distribution is out of the design space (i.e., the functional is not 0 at the minimum). The pressure distribution p^* is obtained with an outlet boundary condition that differs from the one that is actually used in the optimization routine. The results are given in Fig. 7.

The SD1 updating strategy had the least attractive rate of reduction of the functional. Our experience showed, nevertheless, that it was the most reliable in cases of complicated surface topologies that can occur in flow fields with embedded shocks. The BFGS2 becomes the most efficient of the algorithms tested when it is coupled with SD1. With this algorithm, the functional was reduced by orders of magnitude.

For the test case of Fig. 4, the central processing unit (cpu) times required on a DEC 3000/500 were as follows:

SD1	4h 08min
SD2	6h 19min
BFGS1	3h 59min
BFGS2	5h 58min

6. CONCLUDING REMARKS

We have derived an expression of the gradient of the cost function with respect to the shape coefficients. The boundary conditions for the costate equations have been presented; we have shown their relevance to the well posedness of the problem. In the case of shocks, we provided the proper conditions for the costate equations at the discontinuity. On the discrete level, we proposed a method of integrating the costate equations in accordance with a revisited scheme. Additional work is needed to test the algorithm with more realistic test cases and to apply the One-Shot method (Ref. [13]) to hyperbolic problems.

APPENDIX I

The Jacobian matrices for the Euler equation in conservative variables are

$$\mathbf{A} = \begin{bmatrix} 0 & 1 & 0 & 0 \\ kV^2 - u^2 & (3-\gamma)u & -2kv & 2k \\ -uv & v & u & 0 \\ -(\gamma e + 2kV^2)u & \gamma e - kV^2 - 2ku^2 & -2kuv & \gamma u \end{bmatrix} \tag{AI.1}$$

$$\mathbf{B} = \begin{bmatrix} 0 & 0 & 1 & 0 \\ -uv & v & u & 0 \\ kV^2 - v^2 & -2ku & (3-\gamma)v & 2k \\ (-\gamma e + 2kV^2)v & -2kuv & \gamma e - kV^2 - 2kv^2 & \gamma v \end{bmatrix}. \tag{AI.2}$$

The Jacobian in the direction $\mathbf{n}$ is $\mathbf{C} = \mathbf{A}n_x + \mathbf{B}n_y$. The left ($\mathbf{L}_n$) and right ($\mathbf{L}_n^{-1}$) eigenvector matrices of $\mathbf{C}$ are

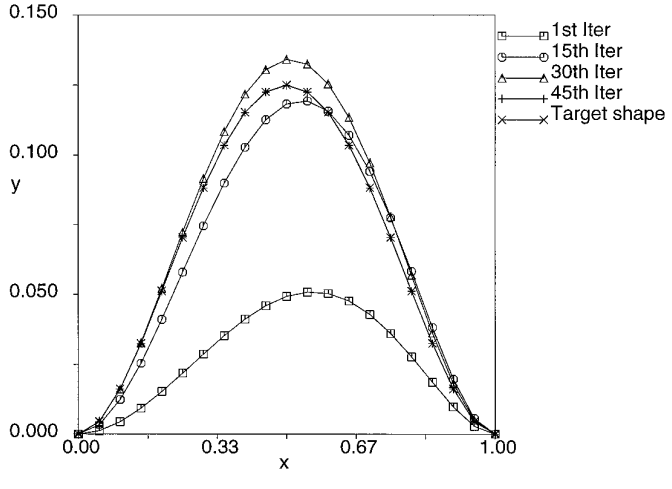

FIG. 6. Wall shapes sequence with BFGS2. Starting configuration: constant section.

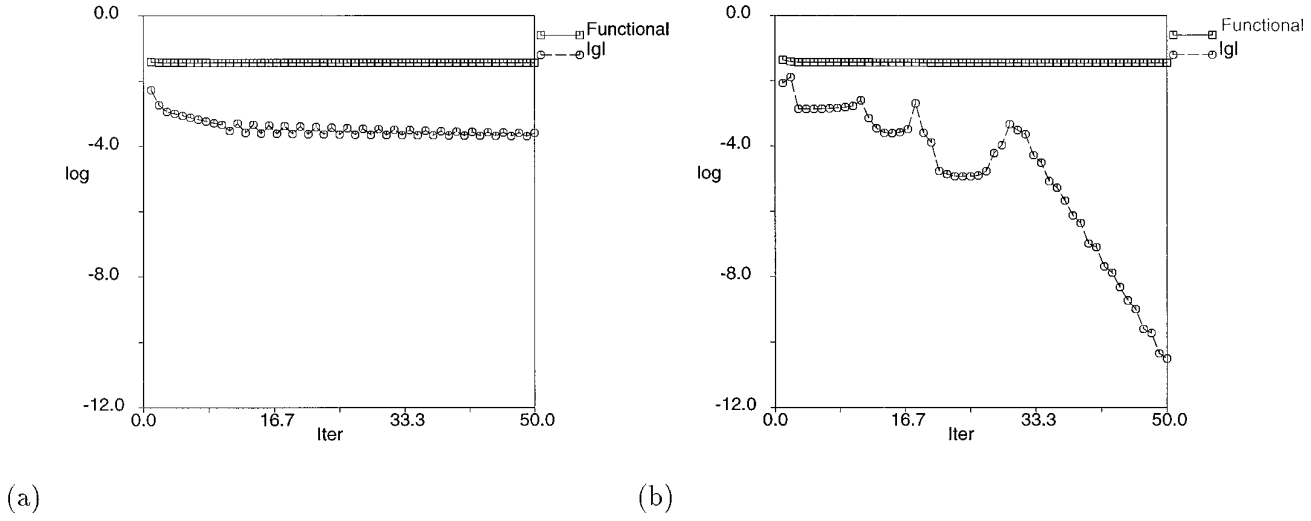

FIG. 7. (a) SD2; (b) BFGS2.

$$\mathbf{L}_n = \begin{bmatrix} 1 - kV^2/a^2 & 2ku/a^2 & 2kv/a^2 & -2k/a^2 \\ V_t/\rho & n_y/\rho & -n_x/\rho & 0 \\ (-V_n + kV^2/a)/\rho & (n_x - 2ku/a)/\rho & (n_y - 2kv/a)/\rho & 2k/\rho a \\ (V_n + kV^2/a)/\rho & -(n_x + 2ku/a)/\rho & -(n_y + 2kv/a)/\rho & 2k/\rho a \end{bmatrix} \tag{AI.3}$$

$$\mathbf{L}_n^{-1} = \begin{bmatrix} 1 & 0 & \rho/2a & \rho/2a \\ u & \rho n_y & \rho(u + an_x)/2a & \rho(u - an_x)/2a \\ v & \rho n_x & \rho(v + an_y)/2a & \rho(v - an_y)/2a \\ V^2/2 & -\rho V_t & \rho(V^2 + a^2/k + 2aV_n)/4a & \rho(V^2 + a^2/k - 2aV_n)/4a \end{bmatrix}, \tag{AI.4}$$

where $V_n = \mathbf{V} \cdot \mathbf{n}$ and $V_t = \mathbf{V} \cdot \mathbf{t}$. The diagonal matrix $\mathbf{D}_n = \mathbf{L}_n \mathbf{C}_n \mathbf{L}_n^{-1}$ is

$$\mathbf{D}_n = \begin{bmatrix} V_n & 0 & 0 & 0 \\ 0 & V_n & 0 & 0 \\ 0 & 0 & V_n + a & 0 \\ 0 & 0 & 0 & V_n - a \end{bmatrix}. \tag{AI.5}$$

APPENDIX II

To calculate $\delta\mathscr{L}_U$, consider the increment $\mathbf{U} \leftarrow \mathbf{U} + \varepsilon\tilde{\mathbf{U}} \Rightarrow$

$$\mathbf{F} \leftarrow \mathbf{F} + \varepsilon\mathbf{A}\tilde{\mathbf{U}} + h.o.t. \quad \text{and} \quad \mathbf{G} \leftarrow \mathbf{G} + \varepsilon\mathbf{B}\tilde{\mathbf{U}} + h.o.t.$$

We obtain

$$\delta\mathscr{L}_U = \int_a^b \frac{\partial p}{\partial \mathbf{U}}\bigg|_\Theta (p^w - p^*)\tilde{\mathbf{U}}\, dx + \int_\Omega {}^t\mathbf{\Lambda}[(\mathbf{A}\tilde{\mathbf{U}})_x + \mathbf{B}\tilde{\mathbf{U}})_y]\, d\Omega + \int_\Theta \mu\mathbf{n} \frac{\partial \rho\mathbf{V}}{\partial \mathbf{U}} \tilde{\mathbf{U}}\, ds + h.o.t. \tag{AII.1}$$

If we apply Gauss's theorem to the second integral of the above equation then we find Eq. (7). Equations (8) and (9) are easily obtained.

To calculate $\delta\mathscr{L}_\alpha$, we first consider the variation of the functions defined on Θ:

$$\alpha_i \leftarrow \alpha_i + \varepsilon\tilde{\alpha}_i \Rightarrow p^w \leftarrow p^w + \varepsilon \frac{dp}{dy} f_i \tilde{\alpha}_i \quad \text{and}$$

$$\rho\mathbf{V} \leftarrow \rho\mathbf{V} + \varepsilon \frac{\partial \rho\mathbf{V}}{\partial y} f_i \tilde{\alpha}_i.$$

Then we consider the variation of the geometry; other

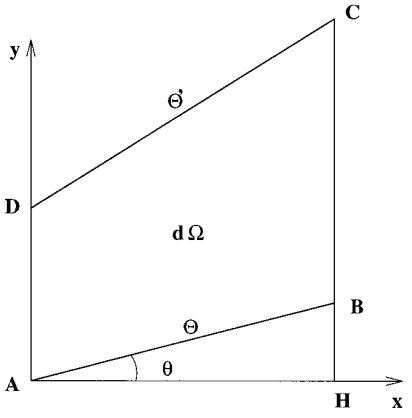

FIG. 8. Variation of the domain of integration Ω. $AH = dx$, $AD = \varepsilon\bar{y}$ and $BC = \varepsilon(\bar{y} + \partial\bar{y}/\partial x\, dx)$.

higher order effects are disregarded. When the geometry is perturbed, the domain of integration Ω, the normal **n** and the element of integration ds are perturbed. The domain Ω is increased (Fig. 8) by a quantity $\varepsilon\tilde{\alpha}_i f_i \cos\theta\, ds$. The normal **n** is perturbed by a quantity $-\varepsilon\tilde{\alpha}_i\, df_i/dx \cos^2\theta \mathbf{t}$; ds, by $\varepsilon\tilde{\alpha}_i\, df_i/dx \cos\theta \sin\theta\, ds$. (See Fig. 9).

APPENDIX III

Consider Eq. (14). This equation defines the boundary conditions for $\mathbf{\Lambda}$ after we impose the proper constraints on $\tilde{\mathbf{U}}$. At the inlet, only one component of the variation of the flux in the direction normal to the boundary $\tilde{\mathbf{F}}_n = (\mathbf{A}n_x + \mathbf{B}n_y)\tilde{\mathbf{U}}$ is independent of the others because total pressure, total temperature, and σ are fixed. If we express all components of $\tilde{\mathbf{F}}_n$ in terms of $\widetilde{\rho u}$ we obtain

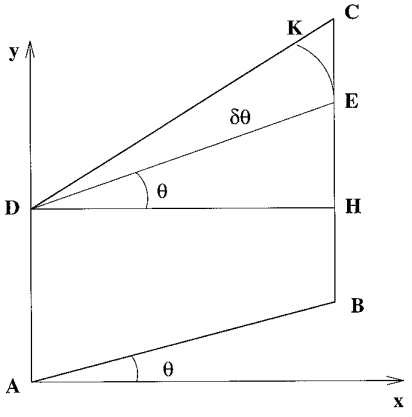

FIG. 9. Variation of **n** and ds. $CE = \varepsilon\partial\bar{y}/\partial x\, dx$, $DH = dx$, $DE = ds$, $\varepsilon\delta\theta = EK/ds$, and $EK = CE\cos\theta$, i.e., $\delta\theta = \partial\tilde{y}/\partial x \cos^2\theta$. The variation of ds is $KC = \varepsilon\partial\bar{y}/\partial x \sin\theta\, dx$.

$$\tilde{\mathbf{F}}_n = \begin{Bmatrix} \xi \\ [\xi + \eta\sigma/(1-M^2)]u \\ [\sigma\xi - \eta/(1-M^2)]u \\ H\xi \end{Bmatrix} \widetilde{\rho u},$$

where $\xi = n_x + \sigma n_y$, $\eta = (n_y - \sigma n_x)$, H is the specific total enthalpy, and M is the local Mach number. For an arbitrary choice of $\widetilde{\rho u}$, from Eq. (14) we have

$$\lambda_1\xi + \lambda_2 u[\xi + \eta\sigma/(1-M^2)] + \lambda_3 u[\sigma\xi - \eta/(1-M^2)] + \lambda_4 H\xi = 0. \tag{AIII.1}$$

At the outlet, if the flow is subsonic, then only the static pressure is fixed; therefore, three components of the vector $\tilde{\mathbf{U}}$ are arbitrary. If we take $\widetilde{\rho e}$ as the dependent variable, we have

$$\tilde{\mathbf{F}}_n = \begin{bmatrix} \widetilde{\rho u}n_x + \widetilde{\rho v}n_y \\ \widetilde{\rho u}(V_n + un_x) + un_y\widetilde{\rho v} - \tilde{p}uV_n \\ \widetilde{\rho v}(V_n + vn_y) + vn_x\widetilde{\rho u} - \tilde{p}vV_n \\ -\tilde{p}(\gamma p/2k\rho + u^2 + v^2) + \widetilde{\rho u}(V_n u + Hn_x) + \widetilde{\rho v}(V_n v + Hn_y) \end{bmatrix}.$$

For an arbitrary choice of $\tilde{p}$, $\widetilde{\rho u}$, and $\widetilde{\rho v}$, from Eq. (14) we have

$$\begin{aligned} \lambda_1 n_x + \lambda_2(V_n + un_x) + \lambda_3 vn_x + \lambda_4(V_n u + Hn_x) &= 0 \\ \lambda_1 n_y + \lambda_2 un_y + \lambda_3(V_n + vn_y) + \lambda_4(V_n v + Hn_y) &= 0 \\ \lambda_2 uV_n + \lambda_3 vV_n + \lambda_4 V_n(\gamma p/2k\rho + u^2 + v^2) &= 0. \end{aligned} \tag{AIII.2}$$

For a supersonic outlet, no conditions exist on $\tilde{\mathbf{U}}$; therefore, we have

$$\mathbf{\Lambda} = \mathbf{0}. \tag{AIII.3}$$

If a shock is embedded in the flow field, then the shock is considered as a boundary for the costate equations. The consequent boundary conditions are applied on each side, i.e., Eq. (AIII.3) before the shock and Eq. (AIII.1) after the shock.

For the upper wall, we have

$$\tilde{\mathbf{F}}_n = \begin{bmatrix} 0 \\ n_x \\ n_y \\ 0 \end{bmatrix} \tilde{p}$$

such that for an arbitrary choice of $\tilde{p}$ Eq. (14) is satisfied if

$$\lambda_2 n_x + \lambda_3 n_y = 0. \quad \text{(AIII.4)}$$

At the lower wall, Eq. (13) applies. Because the rank of $\mathbf{A}n_x + \mathbf{B}n_y$ at the wall is 2, the system has only two linearly independent rows. We obtain

$$\lambda_2 n_x + \lambda_3 n_y + (p^w - p^*) \cos \theta = 0, \quad \text{(AIII.5)}$$

which is the boundary condition for $\mathbf{\Lambda}$, and

$$\mu = -[\lambda_1 + u\lambda_2 + v\lambda_3 + (\gamma e - kV^2)\lambda_4], \quad \text{(AIII.6)}$$

which is the relation between μ and $\mathbf{\Lambda}$ on the boundary.

ACKNOWLEDGMENTS

Many discussions with S. Ta'asan and M. Pandolfi contributed to the formulation of the problem and to its numerical solution.

REFERENCES

1. F. Beux and A. Dervieux, *Finite Elements Anal. Design*, **12,** 281 (1992).
2. J. Borggaard, J.A. Burns, E. Cliff, and M. Gunzburger, Technical Report 93-13, ICASE, 1993 (unpublished).
3. R. Fletcher, *Practical Methods of Optimization*, Vol. I (Wiley, New York, 1980).
4. A. Harten, B. Engquist, S. Osher, and S. R. Chakravarthy, *J. Comput. Phys.* **71,** 231 (1987).
5. A. Iollo, M.D. Salas, and S. Ta'asan, Technical Report 93-78, ICASE (1993); and in *Proceedings, 14th ICNMFD*, Lecture Notes in Physics (Springer-Verlag, Berlin/New York, 1995).
6. A. Jameson. Technical Report 88-64, ICASE, 1988 (unpublished).
7. M. J. Lighthill, *ARC Rand M 2112* (1945).
8. J. L. Lions, *Optimal Control of Systems Governed by Partial Differential Equations* (Springer-Verlag, Berlin, 1971).
9. A. Miele, *Theory of Optimum Aerodynamic Shapes* (Academic Press, New York, 1965).
10. G. Moretti, *Comput. and Fluids* **7,** 191 (1979).
11. G. Moretti, Computation of flows with shocks, *Annu. Rev. Fluid Mech.*, **19** (1987).
12. M. Pandolfi, A contribution to the numerical prediction of unsteady flows, *AIAA J* **22** (1984).
13. S. Ta'asan, G. Kuruvila, and M.D. Salas, in *30th Aerospace Sciences Meeting and Exhibit*, AIAA 92-005 (Jan. 1992).